JOC The Journal of Organic Chemistry

Article

pubs.acs.org/joc

Regioselective Internal Carbonylation of the 2-Aza-21-carbaporphyrin: Access to Configurationally Stable Chiral Porphyrinoids

Bin Liu,[†] Xiaofang Li,*[,†] Justyna Maciołek,[‡] Marcin Stępień,[‡] and Piotr J. Chmielewski*[,‡]

[†]Key Laboratory of Theoretical Chemistry and Molecular Simulation of Ministry of Education, Hunan Province College Key Laboratory of QSAR/QSPR, School of Chemistry and Chemical Engineering, Hunan University of Science and Technology, Xiangtan, Hunan 411201, China

[‡]Department of Chemistry, University of Wrocław, 14 F. Joliot-Curie Street, 50 383 Wrocław, Poland

Supporting Information

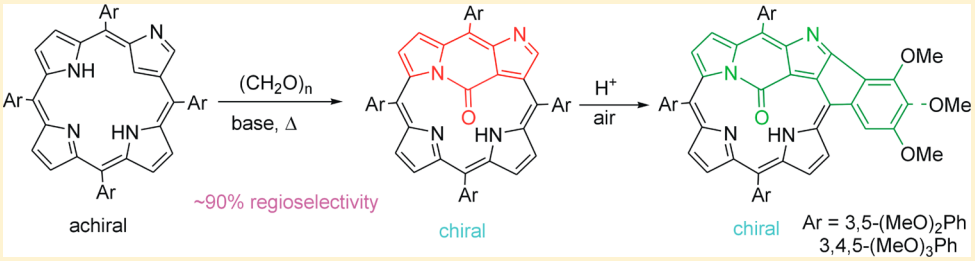

ABSTRACT: Reaction of paraformaldehyde with *meso*-tetraaryl-2-aza-21-carbaporphyrins (NCP) in the presence of a basic catalyst afforded fused lactam derivatives comprising a >C═O bridge linking the internal carbon C21 with one of the internal nitrogens. The isomer **2** with C21−C(O)−N24 bridge is formed with about 9-fold molar excess over that with C21−C(O)−N22 bridge (**3**). The ^{1}H NMR and UV−vis spectral characteristics indicate aromatic character of the derivatives. For *meso*-tetrakis(3′,5′-dimethoxy)- and *meso*-tetrakis(3′,4′,5′-trimethoxy)-21,24-carbonyl-NCP an efficient external ring fusion by linking C3, i.e., the external carbon of the *confused* pyrrole, with an ortho carbon of the adjacent aryl was observed under acidic conditions, yielding derivatives **4c** and **4d**, comprising a linear system of five fused rings. The chirality and configurational stability of these carbonylated systems were established by a chiral stationary phase HPLC and circular dichroism. The interaction of **2** with chiral acids and alcohols leading to the formation of diastereomers was observed by ^{1}H NMR. Slow racemization of **2** under acidic conditions was established by HPLC and ^{1}H NMR and a mechanism for this process was proposed.

INTRODUCTION

Porphyrinoids, the oligopyrrolic aromatic macrocycles, are ubiquitous in basic and applied chemistry owing to their versatile redox, acid−base, optical, and coordination properties.[1−9] Their reactivity is also attractive, allowing fine-tuning of the properties of the system or profound modification of the structure without destruction of the macrocyclic ring. 2-Aza-21-carbaporphyrin[10−12] **1**, also known as N-confused porphyrin (NCP), takes a special part among porphyrin derivatives, analogues, and homologues;[13−17] since its synthesis is facile, and further modifications of the preformed macrocycle are relatively simple by virtue of the *confused* pyrrole that possesses three sites of different reactivity (2-N, 3-C, and 21-C), and each of them can be a target of substitution or addition reactions. In our search for new chiral macrocyclic systems based on the NCP ring,[18−26] we have turned our attention to the reaction that takes place between **1** and formaldehyde under basic conditions that leads to the macrocycle with the interior fused by a carbonyl group. There are several derivatives known already comprising a bridge between atoms of the internal porphyrin core of NCP[27−31] that were obtained as products of multistep processes. The present system can be obtained by one-pot regioselective synthesis gaining configurational stability of the chiral porphyrin ring and retaining its macrocyclic aromaticity.

RESULT AND DISCUSSION

Synthesis and Characterization. The reaction was conducted at elevated temperatures under nitrogen atmosphere with a 10-fold molar excess of paraformaldehyde over NCP (Scheme 1) in the presence of various bases, though only a relatively strong organic proton scavenger resulted in the formation of **2** (see Supporting Information, Table S1). The best results were obtained for triethylamine as a base in refluxing toluene as a solvent. Under these conditions, about 60% conversion after 20 h of the reaction time and more than 40% of overall yield of **2** upon isolation were observed. The effectiveness of the reaction is thus relatively low, but the porphyrin reactant does not undergo decomposition to a considerable degree and the product is easily separable from

Received: February 4, 2014
Published: March 6, 2014

   dx.doi.org/10.1021/jo500272t | J. Org. Chem. 2014, 79, 3129−3139

Scheme 1

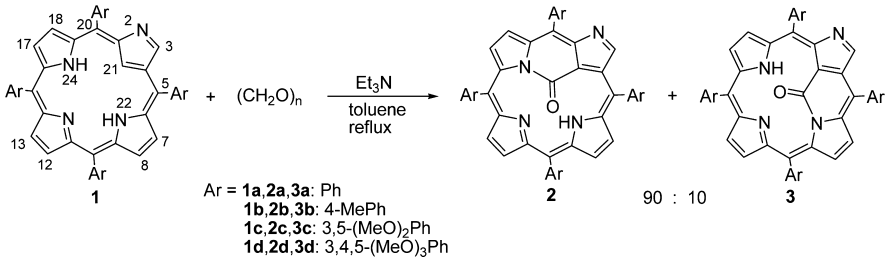

the starting NCP by column chromatography. Formation of two isomeric products was established on the basis of ^{1}H NMR of a reaction mixture, and their molar ratio was about 10:1 by signal integration. As it may be expected, the chromatographic migration rates of the isomers are very close; thus, application of preparative TLC and/or HPLC techniques was needed to separate **2** from **3**. Low content of the minor isomer **3** caused its loss upon separation, preventing detailed characterization which was thus confined to the observation of its presence in the mixtures with the major isomer **2**. The high-resolution mass spectrometry for **2b** (m/z 697.2973; calc. for $[C_{49}H_{37}N_4O]^+$ (M +H), 697.2962) indicated attachment of the carbonyl group to the porphyrin ring that was accompanied by a loss of two hydrogen atoms of the original **1b**. The same mass changes were also observed starting from porphyrins **1a**, **1c**, and **1d**. The optical spectra showed a considerable blue shift of Q bands (10−50 nm) with respect to those of the starting porphyrin, but the spectral pattern indicated that the system retained its aromaticity (Figure 1). The emissive properties are more pronounced for **2**

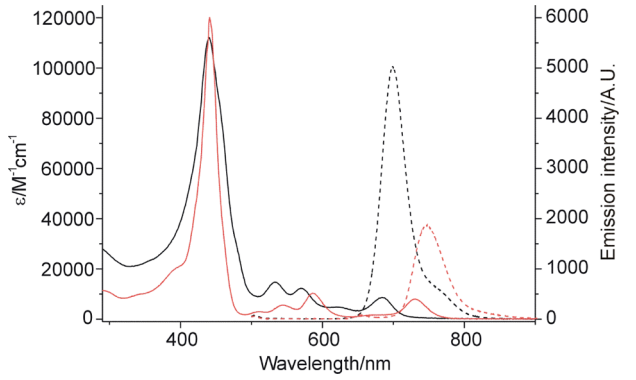

Figure 1. Absorption (solid lines) and emission (dashed lines, excitation at 439 nm) spectra of **2b** (black traces) and **1b** (red traces) in toluene at room temperature.

than for the starting porphyrin **1**, and the determined fluorescence quantum yields Φ_F at room temperature in toluene solutions are 0.12 and 0.04 for **2b** and **1b**, respectively. The value of Φ_F for **2b** is close to that observed for regular *meso*-tetraphenylporphyrin.[32,33]

^{1}H NMR of **2** is in line with the aromatic character of the product with the pyrrole signals spread over the region of δ 8.2−8.8 ppm. In the high-field part of the spectrum, however, there is no signal of 21-H which indicates internal carbon C21 as a target of substitution, and the only signal in this region is that of one internal NH (δ −0.35 ppm, $CDCl_3$, 213 K) that can be assigned on the basis of its correlation with a pair of the pyrrole protons 7-H, 8-H in the low-temperature COSY experiment (δ 8.83, 8.74 ppm, 213 K). Somewhat nontypical is the position of a proton at C3 whose signal appears at about δ 9.6 ppm that could be misinterpreted as an indication of the presence of an aldehyde group. The GIAO calculations of the NMR spectra for the DFT-optimized structure of **2b** (Figure 2) afforded assignment of this

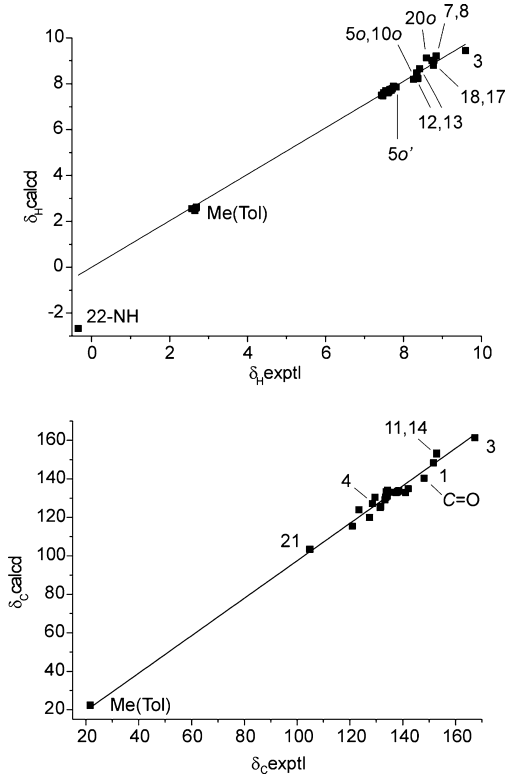

Figure 2. Correlations of experimental and calculated chemical shifts of proton (top) and selected carbon-13 (bottom) NMR signals of **2b**.

signal to the external proton of the *confused* pyrrole (3-H), while chemical shift of C═O was predicted at δ_C 140.4 ppm, i.e., strongly upfield with respect to the value which could be anticipated for the amide carbon (about δ_C 165 ppm). The predicted value is in line with observation of a weak correlation of 3-H with a carbon resonating at δ_C 147.9 ppm in the HMBC experiment ($CDCl_3$, 213 K), apart from four other heteronuclear correlations of this proton at δ_C 167.3 (C3), 151.7 (C1), 127.5 (C4), and 104.6 ppm (C21). The other proton signals were assigned on the basis of 2D experiments at low temperature (213 K, $CDCl_3$) allowing position identification of the proton-bearing nitrogen as N22, and thus, involvement of N24 in the internal ring formation in the major reaction product. The compound is nonplanar which can be inferred from magnetic inequality of the ortho- or meta-protons belonging to each of the aryl substituents observed at low temperature when rotation about the *meso*−*ipso*

dx.doi.org/10.1021/jo500272t | J. Org. Chem. 2014, 79, 3129−3139

bonds is slow at the NMR time scale. At room temperature some of the ortho proton signals are broadened and coalesced due to a faster rotation.

Analysis of the X-ray diffraction of the single crystal of **2b** reveals the presence of one carbonyl bound to two atoms of the porphyrin interior, being in the cis orientation to each other (Figure 3). Formation of a six-membered ring that is fused with

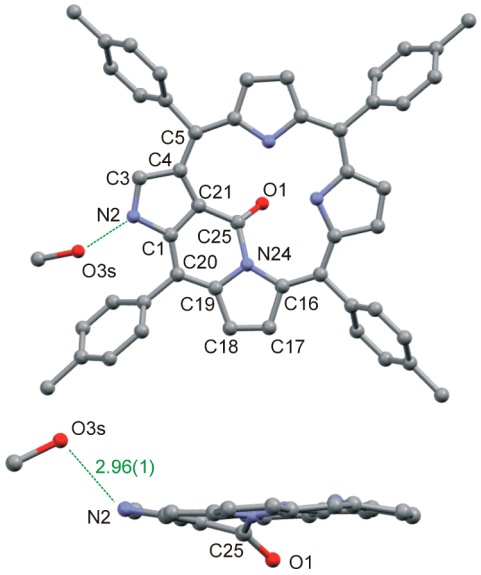

Figure 3. Perspective views of the molecular structure of **2b**: top, front view; bottom, side view. Only one out of two sites of the CO group is shown which are equally occupied due to a disorder. All hydrogens are omitted. In the side view, all tolyl substituents are omitted for clarity.

two pyrroles is thus apparent. The C25−O1 distance of 1.207(9) Å indicates a double bond, while the C25−N24 and C25−C21 distances are typical for single bonds (1.553(8) and 1.533(8) Å, respectively) in accordance with the formulation of this fragment as a cyclic amide. The CO moiety is disordered over two equally populated sites and only half of the molecule appears in the asymmetric unit; thus, the unequivocal assignment of atoms to particular sites is not straightforward when macrocyclic rings are concerned. Some support for the site assignment came from the interaction of **2b** with a co-crystallized solvent present in the crystal lattice. A molecule of methanol disordered over three sites can be found in close contact with one of the atoms of **2b**, and thus, this site was assigned to N2 interacting with the hydroxyl group of the alcohol by H-bonding (N2−O4s 2.71(2) Å, N2−O3s 2.96(1) Å). Similar association of the MeOH molecule with the nitrogen of the *confused* pyrrole has been observed in the crystal structure of bis(NCP)[34] as well as in some sandwich-type lanthanide complexes of NCP and phtalocyanine.[35] The macrocyclic ring is essentially planar with 0.1 Å of average deviation from the mean plane defined by all 24 non-H ring atoms, while the CO moiety lies under the plane with deviations of 0.68 Å for C25 and 1.40 Å for O1. The carbonyl group is sterically locked on one side of the macrocycle and cannot be threaded through its interior; thus, the system is configurationally stable and its faces are permanently differentiated. Considering the pro-chiral character of the NCP ring, such a nonplanar structure of the molecule causes its chirality, although due to the disorder of the molecule in the crystal lattice, the distinction of the enantiomers is not possible.

Redox Properties. Redox properties of **2b** were examined by means of cyclic and squarewave voltammetry indicating two reversible reductions at −1305 and −1720 mV and three irreversible oxidation processes at 637, 889, and 1067 mV (Figure 4; all potentials referenced with a ferrocene/ferrocenium

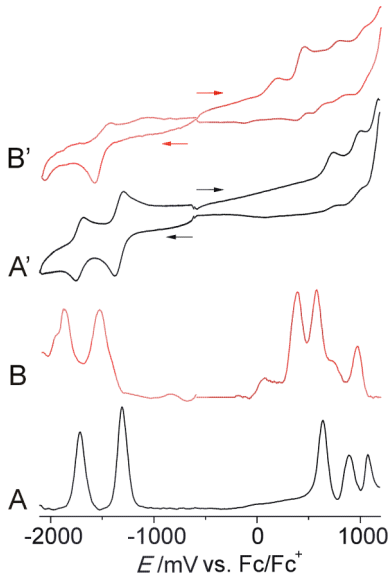

Figure 4. Squarewave voltammetry of **2b** (A) and **1b** (B) and cyclic voltammetry of **2b** (A′) and **1b** (B′) in dichloromethane.

couple as an internal standard). The electrochemical waves of both reductions and all oxidation processes are anodic shifted with respect to those observed for starting porphyrin **1b** reflecting higher "oxidation state" and resistibility toward oxidation of the internally CO-fused macrocycle. The first reduction of **2b** occurs at the potential that is 200 mV higher than that of **1b**, but its value still indicates a porphyrin anion radical formation rather than reduction of the carbonyl group. In fact, our attempt to deoxygenate **2b** by means of sodium borohydride in THF in the presence of weak organic acids at room temperature[36] resulted in a purple-red solution containing several non-aromatic species. The spectral characteristics of these presumably phlorin-type systems include lack of the intense Soret band in the optical spectrum as well as strongly downfield shifted NH signals (δ 9−11 ppm) and β-pyrrole proton resonances appearing in the region of δ 5−7 ppm in the ^{1}H NMR spectrum (Figure S29). Apparently, the hydrogenation lacked regioselectivity yielding a mixture of nonaromatic products which was readily and almost quantitatively reoxidized to **2b** upon exposure of the reductant-free solution to air for two days.

External Fusion. The internal fusion does not prevent the formation of an externally fused ring involving C3 and an ortho carbon of the 5-aryl. For the systems comprising *meso*-aryls with electron-donating methoxy groups, which activate ortho-positions, the C3−C5*o* bond formation is facile.[37] It was already accomplished after 30 min of reflux in toluene for **2c** or **2d** acidified with trifluoracetic acid, and the conversion into **4c** or **4d** was practically quantitative (Scheme 2). The transformation was combined with a color change from olive green to purple, and after deacidification, the solution turned deep red. The electronic spectrum of **4** is considerably different from the porphyrin-like spectrum of the starting **2** and similar to that of externally 3,5*o*-fused porphyrin **5** with no internal ring fusion[37] (Figure 5). Mass

dx.doi.org/10.1021/jo500272t | J. Org. Chem. 2014, 79, 3129−3139

Scheme 2

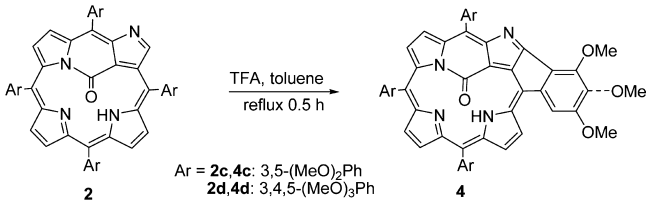

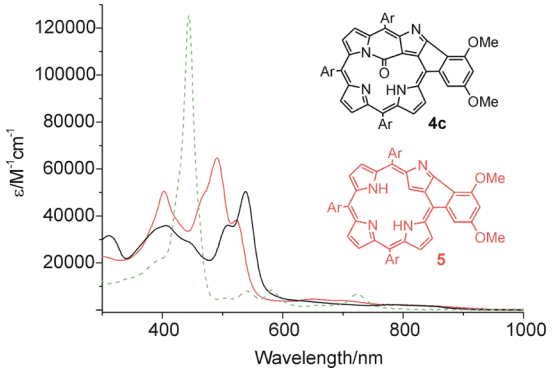

Figure 5. Optical spectra of **4c** (black trace), **5** (red trace), and **1c** (green dashed line) in chloroform.

spectra of **4** indicate the loss of two hydrogens upon reaction. The ^{1}H NMR shows no signal of 3-H and the number of ortho-proton signals is reduced by one, unequivocally indicating reaction sites. In the high-field region of the spectrum, there is only one signal (δ 0.76 ppm for **4c**) that can be assigned to 22-NH, in line with the occupation of C21 and N24 by the CO bridge. The low-temperature COSY spectrum (213 K, $CDCl_3$) showed correlation between the signal of 22-NH at δ 0.57 ppm and a pair of doublet of doublets of β-pyrrole protons at C7 and C8 (δ 8.87 and 8.56 ppm, respectively). In the NOESY spectrum ($CDCl_3$, 233 K), 7-H correlates strongly with a doublet of the 5-o'-H, i.e., proton at the ortho position of the aryl fused with the *confused* pyrrole. Analogously to the parent compounds **2c**, the ortho protons are magnetically distinct due to a nonplanar character of **4c** and some restrictions in the rotation freedom of the *meso*-substituents, while for the effectively flat **5** a pairwise degeneration of the ortho signals has been observed.[37] The macrocyclic aromaticity of **4** is less affected by the external ring fusion compared to the internally nonbridged system **5**. It is reflected by relatively small upfield shift of the pyrrole proton signals resonating in the region δ 7.8−8.8 ppm in **4** with respect to their position in **2** (δ 8.3−8.9), while in the case of **5**, pyrrole signals appeared in a region of δ 7.6−8.2 ppm. Also, the position of the internal NH is less shifted downfield compared to those of 22,24-NH in **5** (δ 1.94, 2.28 ppm).[37]

Separation of Enantiomers and Optical Activity. We succeeded in the separation of the enantiomers of **2b** and **4c** by means of a chiral-phase HPLC column, and their optical activities were determined by the circular dichroism spectra (Figure 6). To assign the absolute configuration, we calculated a CD spectrum by means of TD-DFT method for the DFT-optimized structure of enantiomer *R* of **2b** (Figure 7). The positive signs of the calculated Cotton effects in the Soret and Q-band region indicate that enantiomer 1, i.e., that contained in a fraction migrating

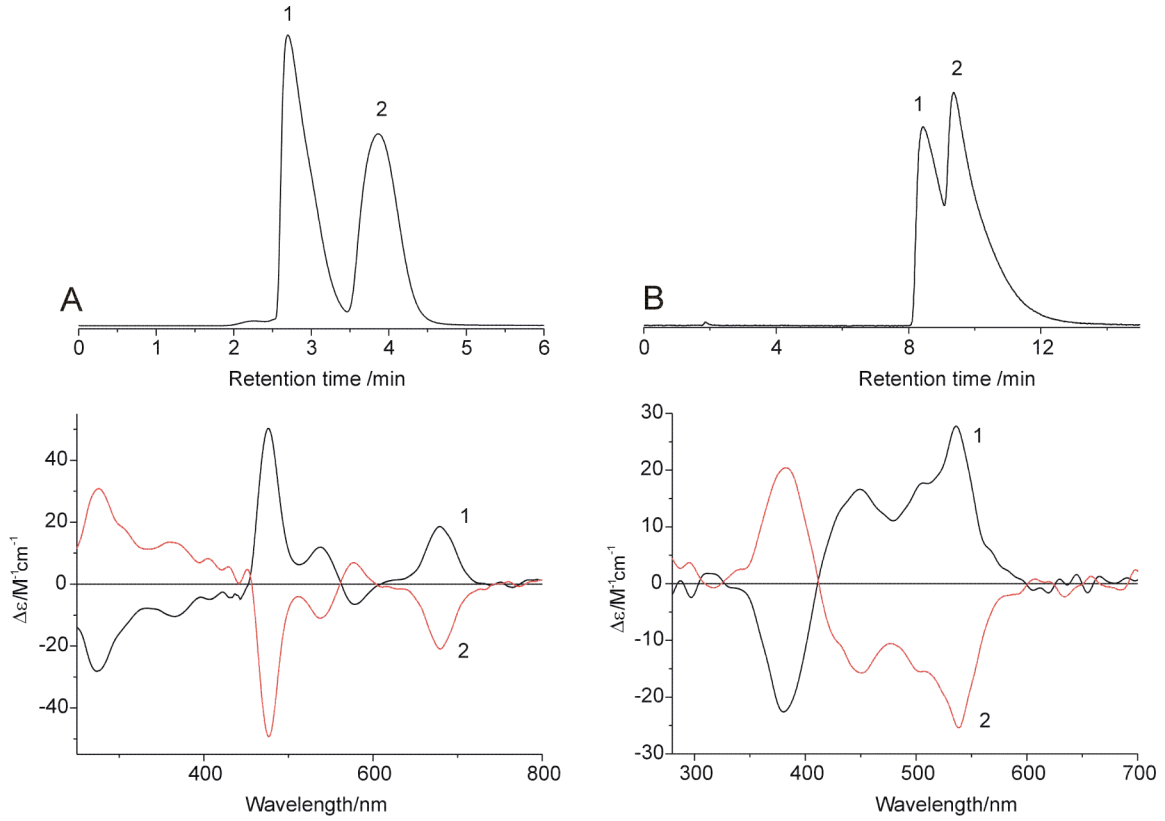

Figure 6. Top: Chiral phase HPLC profiles of **2b** (A, dichloromethane/ethyl acetate 70/30, 2 mL/min, Chirex column 0.46/25 cm, detector wavelength 440 nm, injection 100 μL, room temperature) and **4c** (B, dichloromethane/ethyl acetate 95/5, 3 mL/min, Chirex column 0.46/25 cm, detector wavelength 536 nm, injection 100 μL, room temperature). Bottom: CD spectra of the enantiomers of **2b** (left) and **4c** (right) in $CHCl_3$.

dx.doi.org/10.1021/jo500272t | J. Org. Chem. 2014, 79, 3129−3139

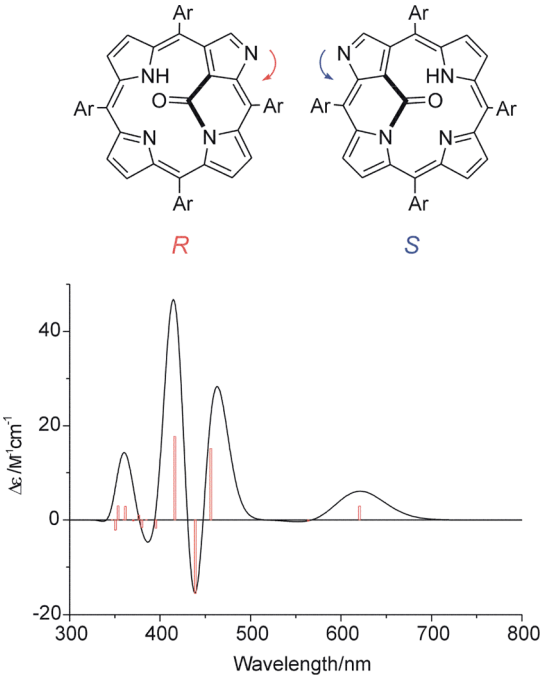

Figure 7. Definition of the absolute configuration of the enantiomers of **2** and CD spectrum calculated for the enantiomer *R*-**2b**.

faster through the chiral stationary phase of the HPLC column (Figure 6), has the absolute configuration *R*.

We attempted to confirm the absolute configuration assignment by the X-ray diffraction method. Unfortunately, the crystal structure obtained from the X-ray diffraction analysis of a crystal consisting of enantiopure **2b**-2, i.e., enantiomer *S*, suffered the same twofold disorder as the racemate (vide supra) and displayed pseudosymmetry with an inversion center within centrosymmetric space group $P2_1/c$.

Chiral Guest Binding. Considering the chirality of **2** and the nucleophilic character of the external nitrogen that can act as an acceptor of hydrogen in H-bonding, we decided to check whether the molecule can be used as a chiral recognition device. The ^{1}H NMR-monitored titration of racemic **2b** with enantiopure (*S*)-camphorsulfonic acid ((*S*)CamSO$_3$H, $CDCl_3$, 213 K) revealed gradual formation of monocationic species within the concentration range of 0−1 equiv of the acid. The incoming proton is attached to the external nitrogen N2, which is reflected by the appearance of a strongly downfield shifted signal near δ 16.1 ppm. Positions of the pyrrole signals are shifted upfield, while the internal 22-NH resonates at δ 1.00 ppm. The most striking feature of the ^{1}H NMR spectrum of [*rac*-**2b**H][(*S*)CamSO$_3$] is doubling of some signals of both the macrocycle and the anion protons indicating formation of diastereomeric adducts, which possess a tight ion-pair character (Figure 8). Significantly, upon addition of (*S*)CamSO$_3$H to the

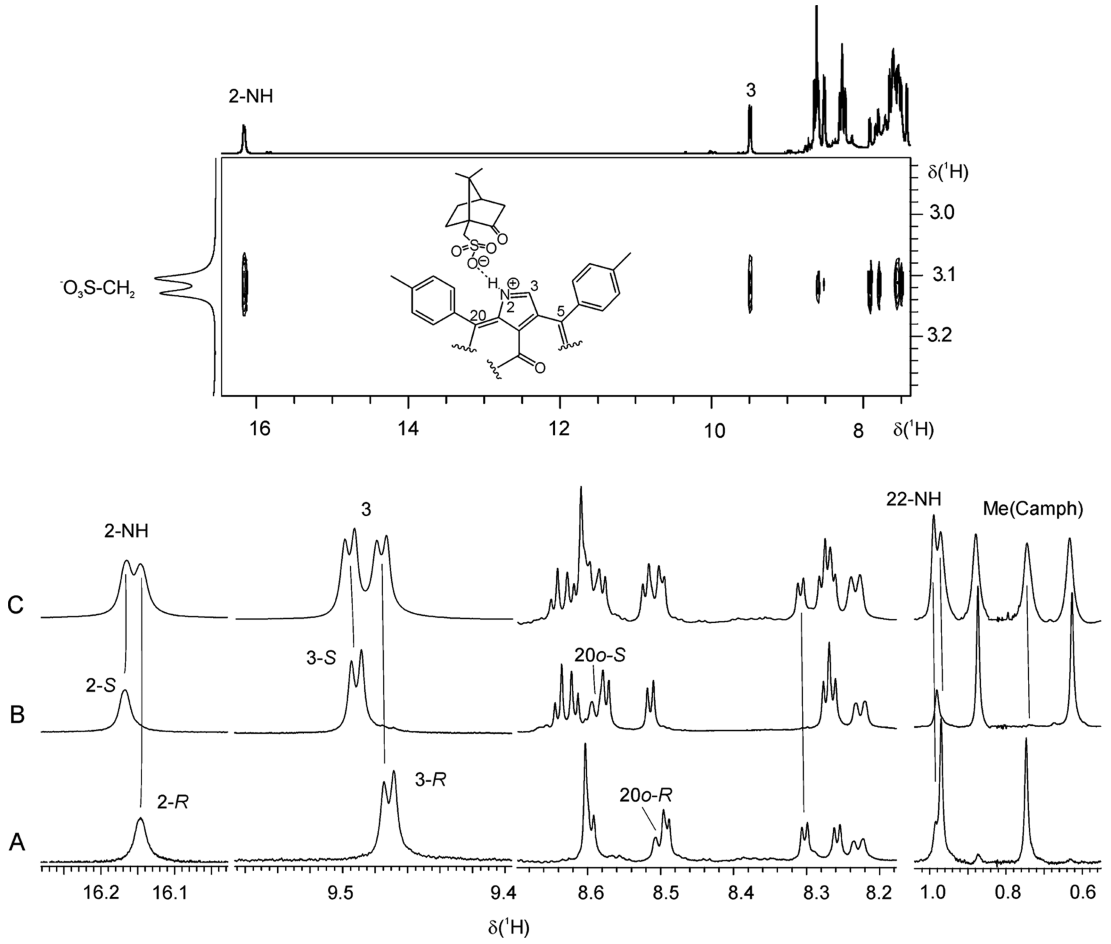

Figure 8. Selected regions of ^{1}H NMR spectra (600 MHz, $CDCl_3$, 213 K) of [*R*-**2b**H][(*S*)CamSO$_3$] (A), [*S*-**2b**H][(*S*)CamSO$_3$] (B), and [*rac*-**2b**H][(*S*)CamSO$_3$] (C). The upper panel presents a fragment of the NOESY map for [*rac*-**2b**H][(*S*)CamSO$_3$], displaying correlations between anion and cation protons.

dx.doi.org/10.1021/jo500272t | J. Org. Chem. 2014, 79, 3129−3139

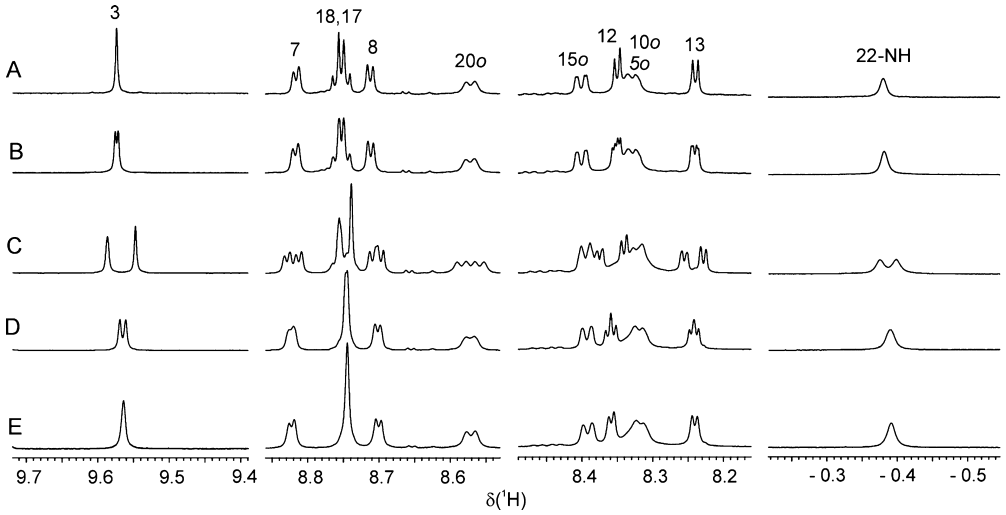

Figure 9. Selected regions of the ^{1}H NMR spectra (600 MHz, $CDCl_3$, 213 K) of **2b** (A) and upon addition of 2.2 equiv 1*R*,2*S*,5*R*-menthol (B), 40 equiv 1*R*,2*S*,5*R*-menthol (C), 40 equiv 1*R*,2*S*,5*R*-menthol and 30 equiv 1*S*,2*R*,5*S*-menthol (D), 80 equiv of racemic menthol (E).

solutions of separated enantiomers of **2b**, formation of distinct species was observed for each enantiomer (Figure 8). The association of the anion and its position with respect to the macrocycle can be inferred from the NOESY spectrum ($CDCl_3$, 213 K). In particular, one of the diastereotopic methylene protons of the $-CH_2SO_3^-$ group of the anion resonating at δ 3.11 ppm gives rise to strong NOE signals with both 3-H and 2-NH as well as with ortho and meta protons of the aryl substituents at *meso* positions 5 and 20, i.e., in the vicinity of the protonation site. At higher concentrations of the acid (1−2 equiv), consecutive formation of a dication $[\mathbf{2b}H_2]^{2+}$ was observed (Figure S32, 213 K, $CDCl_3$) involving internal nitrogen N22 as a second protonation site. This new form gave rise to a more downfield shifted 2-NH signal at δ 17.60 ppm, while some signals due to the associated anion appeared in the region −1.55−0 ppm. That indicated the position of the guest over the macrocyclic ring, i.e., in the area of shielding influence of the aromatic current, hence in close contact with the internal NH groups. Clearly, also dication $[\mathbf{2b}H_2]^{2+}$ interacts with $CamSO_3^-$ which results in the formation of diastereomers upon addition of enantiopure acid to racemic **2b**. Due to an equilibrium between the protonated and nonprotonated species that seemed to be fast in the NMR time scale, neither the effects related to the protonation nor to the adduct formation was observed at room temperature at the lower acid concentration limit (0−1 equiv). On the other hand, at higher concentrations of the acid (2−4 equiv) a splitting of some of the signals was observed when enantiopure (*S*)$CamSO_3H$ was added to *rac*-**2b** at 300 K, though the low-field signal of 2-NH was still absent in the spectrum. No such diastereomeric differentiation occurred upon addition of racemic mixture of the acid (*rac*-$CamSO_3H$) to *rac*-**2b** or to enantiopure *R*-**2b** suggesting an enantioselectivity of the ion-pair formation. In the former case, each enantiomer of the anionic guest discriminates between the enantiomers of the host and interacts solely with one preferred isomer, which results in the formation of enantiomeric mixture. In the latter case, the preference of the host may lead to the formation of adduct with only one enantiomer of the anion. Thus, in this case the pair of diastereomers can be observed by ^{1}H NMR within the fast chemical exchange limit exclusively when an enantiopure guest is added to the mixture of enantiomers of the host.

For a system obtained by the addition of *S*-mandelic acid to *rac*-**2b**, formation of two diastereomeric forms was apparent in the $CDCl_3$ solution at 300 K already in the presence of 1 equiv of the acid (Figure S33). The effect of differentiation of the chemical shifts of diastereomers was more pronounced at lower temperatures down to 233 K, when signals started to broaden. Even at 213 K, however, there was no sign of the cationic form with the externally protonated *confused* pyrrole. Considering very small changes of chemical shifts of the porphyrin upon addition of the *S*-mandelic acid, it can be concluded that in this case the proton transfer to N2 is rather insignificant, and interaction between neutral molecules takes place. This interaction is enantioselective, since upon addition of the racemic mixture of mandelic acid to the solution of *rac*-**2b**, the presence of only one species can be observed by ^{1}H NMR indicating formation of enantiomeric mixture of adducts instead of diastereomers (Figure S33). In the case of another chiral carboxylic acid, namely, 2-(*S*)-bromopropionic acid, effects of the proton transfer toward the porphyrin and tight ion-pair formation was observed, i.e., shift and broadening of the signals. Formation of diastereomers resulted in splitting of some signals, both at room temperature and at 243 K at 10-fold molar excess of the acid, though this effect was rather weak and limited to pyrrole protons 7 and 8 (Figure S34). No interaction of **2b** with L-proline took place even though the presence of the amino acid in the solution was observed in an amount of about 1 equiv at 213 K. In contrast, the effect of diastereomeric differentiation of signals at room temperature was apparent upon shaking the solution of **2b** with solid (*S*)-malic acid, despite its insolubility in chloroform (Figure S35).

Observation of the effective binding of the weak hydroxyacids by **2** directed our attention to chiral alcohols. In the case of enantiopure 2-(*S*)-butanol, the effects related to the interaction with **2b** were not observed, even after addition of 20 equiv of the alcohol. On the other hand, formation of diastereomers was apparent for 1-(*S*)-phenylethanol at 213 K in $CDCl_3$, though the differentiation of the peak positions was rather weak (Figure S36). A much more pronounced effect of the interaction of **2b** with the chiral alcohol molecule was observed in the case of enentiopure 1*R*,2*S*,5*R*-menthol, likely due to the bigger overall size of the guest molecule, though it can be observed only at low temperatures. The differentiation of peak positions depends on

dx.doi.org/10.1021/jo500272t | J. Org. Chem. 2014, 79, 3129−3139

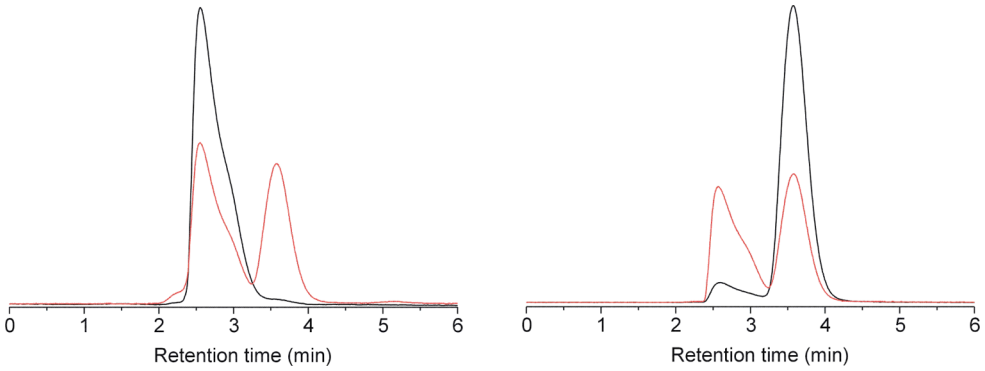

Figure 10. Superimposed chiral phase HPLC profiles of the solutions of *R*-**2b** (left, black trace) or *S*-**2b** (right, black trace) with those of enantiomer mixtures (red traces) obtained upon heating the former solutions with TFA (10 equiv) for 16 h in $CHCl_3$. Conditions: mobile phase, dichloromethane/ethyl acetate 70/30; flow rate, 2 mL/min; Chirex column 0.46/25 cm; detector wavelength, 440 nm; injection, 100 μL; room temperature.

the amount of chiral alcohol added to a certain concentration limit ($\Delta\nu$ = 23.5 Hz at 40 equiv for 3-H at 213 K for $CDCl_3$ solution) indicating rather small value of the binding constants. We did not attempt to estimate these constants since the spectral alterations caused by the addition of the guest are minute. As it was in the case of chiral acids, the binding of menthol is enantioselective; consequently, upon mixing of *rac*-**2b** with racemic menthol there is no differentiation of the signal positions, since diastereomers are not formed and chemical shifts of the ^{1}H NMR signals are practically unaltered with respect to that of the pure host (Figure 9). The separation of signals of the diastereomers depends thus on the contents of the mixture of enantiomeric alcohols which may be used for estimation of the composition of non-racemic systems. Analogous spectral effects related to the association were observed upon addition of another terpenoid, namely, 1-endoborneol. Although apparently the interaction of this alcohol with **2** was weaker than in the case of menthol (for 3-H $\Delta\nu$ = 7.7 Hz at 160 equiv of 1-(*S*)-*endo*-borneol, $CDCl_3$, 213 K), it was enantioselective since the differentiation of signals is diminished upon addition of the 1-(*R*)-*endo*-borneol and was absent when racemic mixture was added (Figure S37).

Racemization. A process of slow racemization in solution was observed upon addition of acid to enantiopure **2b**. By heating a solution of separated enantiomers with 10 equiv of TFA for 20 h at 90 °C in toluene or for 16 h at 60 °C in chloroform, optically inactive mixtures were obtained, in which almost equal contents of both enantiomers were determined by a chiral stationary phase HPLC (Figure 10). For non-acidified solutions containing either of the enantiomers, no significant increase of the antipode concentration was observed even after 40 h of heating.

The guest−host interaction with chiral acid allowed monitoring of the configuration changes by means of NMR. After keeping a $CDCl_3$ solution containing *R*-**2b** and 2.5 equiv of (*S*)$CamSO_3H$ for four weeks at room temperature, racemization resulted in formation of diastereomers, and their molar ratio, d.r., calculated on the basis of ^{1}H NMR signal integration was 1:3.8. Higher acid content accelerated the racemization, and upon addition of 8 equiv of (*S*)$CamSO_3H$, d.r. increased to 1:2 after another week in solution at room temperature. A complete racemization was observed after 22 h when solution was heated to 60 °C. Formation of the racemic mixture was observed also upon heating of the solution of *S*-**2b** with 4 equiv of (*S*)$CamSO_3H$. No NMR spectral changes were observed when solutions containing *rac*-**2b** and 4 equiv of (*S*)$CamSO_3H$ or *rac*$CamSO_3H$ were heated for such a period of time (Figure 11).

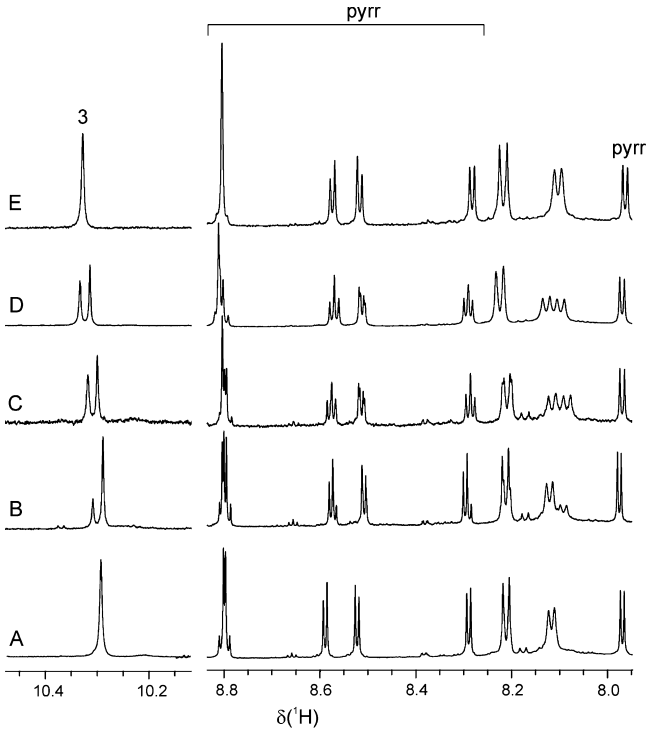

Figure 11. Low-field regions of the ^{1}H NMR spectra of **2b** (500 MHz, 300 K, $CDCl_3$) indicating enantioselective interaction with camphorsulfonic acid and racemization of the macrocycle: (A) *R*-**2b** + (*S*)$CamSO_3H$ (4 equiv); (B) *R*-**2b** + (*S*)$CamSO_3H$ (4 equiv) after four weeks at room temperature; (C) the same solution as in (A), after 22 h of heating at 60 °C, (D) *rac*-**2b** + (*S*)$CamSO_3H$ (4 equiv); (E) *rac*-**2b** + *rac*$CamSO_3H$ (4 equiv).

Racemization,[21,26] inversion of configuration,[25] or chiral induction[20,21,25] have been observed previously for several NCP derivatives in addition to many cases of configurationally stable monomers or dimers.[18,22−24] In all but one[25] system displaying a configuration change, the process was apparently connected merely with more or less energetically accessible structural alteration of the most stable structure and did not involve C−C, C−O, or C−N bond cleavage. The occurrence of racemization in the case of **2b** suggests the availability of an endothermic process facilitating rearrangement of the macro-

dx.doi.org/10.1021/jo500272t | J. Org. Chem. 2014, 79, 3129−3139

cycle interior regarding the position of the C═O group with respect to the mean plane of the ring resulting in configuration change. In Figure 12, both configurations of **2** are shown by

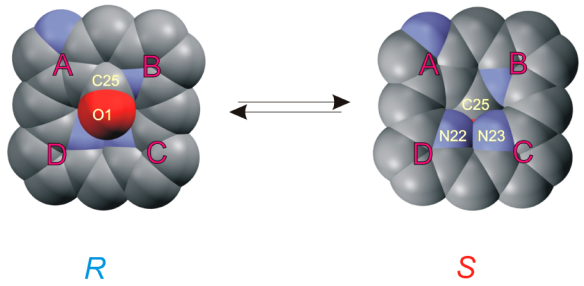

Figure 12. CPK representations of back and front projections of enantiomers of **2** upon inversion of their configurations. The *meso*-substituents and hydrogens are omitted for clarity.

means of a CPK representation of the molecular structure of the enantiomers to illustrate the situation of the carbonyl group within the macrocyclic interior. It is apparent that configuration alteration is not conceivable without a profound change of the porphyrin structure in the transient species which may involve deoxygenation of C25, a considerable deformation, or breaking of the porphyrin ring. A distortion of the regular part of the macrocycle causing both pyrrole C and D to be sharply tipped out of the porphyrin plane to the direction opposite to that of the CO moiety may allow a passage of C25 through the porphyrin interior, though it is unlikely to achieve a transition of the carbon bearing oxygen attached to it. In the presence of an excess of acid, the internal nitrogens N22 and N23 are protonated, which may lead to such a deviation from planarity caused by steric overcrowding. On the other hand, 22,23-NHs seem to constitute an additional obstacle in the course of the CO substituent advancing the other side of the macrocycle. In line with the observation that the racemization is triggered/accelerated by the presence of acid and with that the carbonyl group is a part of a cyclic amide moiety, we propose for the racemization of **2b** a mechanism analogous to the tetrahedral route $A_{AC}2$ established for the acid-catalyzed hydrolysis of amides[38−40] (Scheme 3). The mechanism includes the rate-determining step of water addition, where H_2O molecule approaches C25 of **2b** from the opposite side of the porphyrin than that occupied by original carbonyl oxygen O1. Thus, after subsequent dissociation of the C25−O1 bond of the transient bis(hydroxy) adduct, the molecule attains a configuration that is complementary to that initially observed. The concentration of water dissolved in the organic solvents used, though very low, appears to be sufficient since water is not consumed in this reaction. There is an analogy of this mechanism to that in a previously observed unidirectional configuration change upon transetherification of 3,21-dialkoxy-NCP that took place on the internal carbon C21. Formation of a transient species of ketal character with two different alkoxy groups bound to C21 located on the opposite faces of the macrocyle accounted for the observed inversion of optical activity.[25] In the present case, however, a stochastic character of the process (i.e., water can approach C25 to both enantiomers with the same probability and all further processes are reversible) resulted in the racemic mixture formation rather than a bulk unidirectional inversion of the molecules' configuration.

Scheme 3

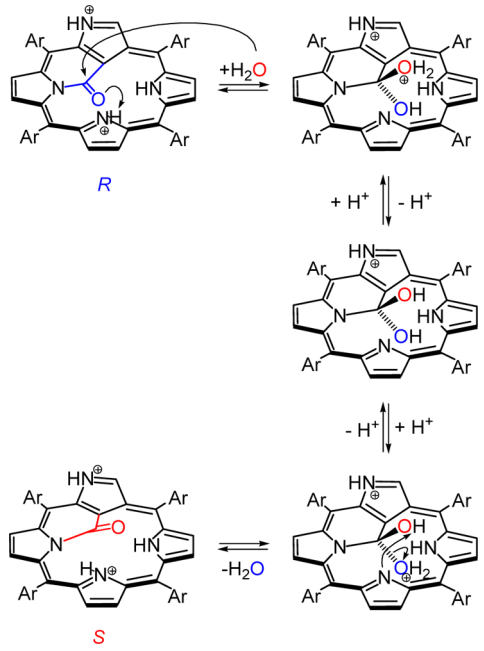

CONCLUSION

Addition of the carbonyl group to the interior of 2-aza-21-carbaporphyrin can be achieved under basic conditions in a direct reaction of the porphyrin and paraformaldehyde, which is likely a source of methylene group that is further oxidized to C═O. The reaction is highly regioselective leading to about 9-fold excess of the major isomer containing the bridge linking C21 with N24. The formed lactam moiety appears to be resistant to reduction and hydrolysis. By a proper choice of *meso*-substituents the unprecedented carbaporpyrinoids comprising a row of five fused rings can be efficiently obtained in an acid-catalyzed reaction of the external carbon of the *confused* pyrrole. The carbonylated systems are chiral and configurationally stable, which allows separation of enantiomers, though slow racemization under acidic conditions is observed. Adducts of **2** or its cations with neutral or anionic chiral guests are formed, exploiting H-bonding in which both external and internal nitrogen sites can be involved. Formation of diastereomers observed for nonracemic mixtures of guest can be potentially useful for estimation of the enantiomer ratio by means of the NMR method in the case of some chiral hydroxyacids or alcohols. Porphyrins with π-bonds delocalized onto polycyclic systems tend to self-assemble by π-stacking even if their macrocyclic ring is not entirely planar,[41] and similar associative behavior has been shown previously for externally fused NCP derivatives.[37] It is thus reasonable to anticipate that compounds consisting of a five fused ring system such as **4** can be, after further derivatization, a promising candidate for the preparation of new materials possessing properties of chiral liquid crystals.

EXPERIMENTAL SECTION

General Methods. All of the reagents from commercial suppliers were used without further purification. All of the solvents were freshly distilled from the appropriate drying agents before use. The analytical TLCs were performed with silica gel 60 F254 plates. Column chromatography was carried out by using silica gel 60 (200−300 mesh ASTM). The NMR spectra were recorded on spectrometers, operating at 500 MHz for ^{1}H and 125 MHz for ^{13}C or at 600 MHz for ^{1}H and 150 MHz for ^{13}C. TMS was used as an internal reference for ^{1}H and

dx.doi.org/10.1021/jo500272t | J. Org. Chem. 2014, 79, 3129−3139

^{13}C chemical shifts and $CDCl_3$ was a solvent. Mass spectrometry measurements were conducted using electrospray ionization technique. Absorption UV−vis spectra and fluorescence spectra were recorded for dichloromethane, chloroform, or toluene solutions. Quantum yields were estimated for toluene solutions in relation to that of tetraphenylporphyrin (Φ_F = 11%)[33] excited at the same wavelength (440 nm). Circular dichroism spectra were obtained at room temperature for chloroform solutions. Resolution of stereoisomers was performed at room temperature by means of Chirex 3010 analytical column (25 cm length, 4.6 mm i.d.) packed with 5 μm silica-gel coated with covalently bound (*S*)-valine and dinitroaniline. Electrochemical measurements were performed for dichloromethane solutions with glassy carbon, platinum wire, and Ag/AgCl as working, auxiliary, and reference electrodes, respectively. The potentials were referenced with ferrocene/ferrocenium couple used as an internal standard.

Calculations. Density functional theory (DFT and TD-DFT) calculations were performed using Gaussian 09.[42] DFT geometry optimizations were carried out in unconstrained C_1 symmetry, using refined X-ray coordinates as starting geometries. DFT geometries were refined to meet standard convergence criteria, and the existence of a local minimum was verified by a normal-mode frequency calculation. DFT calculations were performed using the hybrid functional B3LYP,[43−45] combined with the 6-31G(d,p)[46,47] basis set. The electronic and CD spectra were simulated by means of time-dependent density functional theory (TD-DFT) for 15 states. For these calculations, the polarizable continuum model of solvation was used (PCM, chloroform). The electronic transitions, UV/vis, and CD spectra were analyzed by means of the GaussSum program.[48] The transitions were convoluted by Gaussian curves with 2000 cm^{-1} and 0.25 eV half line widths for the UV/vis and CD spectra, respectively.

Syntheses of Precursors. Starting porphyrin **1a** was obtained by means of the synthetic procedure described by Lindsey for tetraphenyl NCP.[12] The other precursors were obtained analogously, but instead of benzaldehyde a tolylaldehyde,[10] 3,5-dimethoxybenzaldehyde,[37] or 3,4,5-trimethoxyaldehyde[49] were used in the syntheses of **1b**, **1c**, or **1d**, respectively.

General Method of Synthesis of 2. NCP **1** (0.1 mmol), triethylamine (1.5 mmol), and paraformaldehyde (1.5 mmol) were dissolved in 25 mL of freshly distilled toluene. The mixture was refluxed for 15 h under nitrogen and then the solvent was removed under vacuum. The residue was passed down a silica gel column with dichloromethane/ethyl acetate mixture (90/10 v/v) as eluent. The first brown colored fraction was collected, followed by removal of solvent to afford desired NCP derivative **2** with some admixture of the isomeric product **3**. The mixture was subjected to preparative TLC on the silica gel plates with dichloromethnane/ethyl acetate (80/20 v/v) as eluent to separate **2** (faster migrating) from **3** (slower migrating), although efforts to obtain the product **3** as a singular species were unsuccessful. The main product **2** was obtained as dark olive or brown powder by precipitation from dichloromethane solution by addition of hexane and dried *in vacuo*. Yields: 34 mg (53%) for **2a**, 33 mg (47%) for **2b**, 44 mg (50%) for **2c**, 52 mg (52%) for **2d**.

Selected Data for ***2a***. ^1H NMR (500 MHz, $CDCl_3$, 298 K) δ = 7.66 (t, *J* = 8.0 Hz, 2H), 7.73−7.81 (m, 12H), 8.13−8.22 (m, 7H), 8.37 (d, *J* = 4.5 Hz, 1H), 8.67 (d, *J* = 5.0 Hz, 1H), 8.75−8.78 (m, 3H), 9.61 (s, 1H); ^{13}C NMR (125 MHz, $CDCl_3$, 298 K): δ = 105.3, 121.1, 121.2, 123.5, 126.8, 127.0, 127.7, 128.2, 128.3, 128.4, 128.5, 128.6, 128.9, 131.4, 131.6, 133.3, 134.2, 134.3, 134.5, 134.8, 135.4, 136.1, 139.2, 139.3, 141.2, 141.7, 153.5, 153.6, 167.4. UV−vis ($CHCl_3$): λ_{max}/nm (log ε) = 439(4.95), 534(3.95), 571(3.90), 620(3.50), 682(3.82). HRMS (ESI-TOF) calc. for $[C_{45}H_{29}N_4O]^+$ (M+H) *m*/*z* = 641.2336. Found 641.2333.

Selected Data for ***2b***. ^1H NMR (500 MHz, $CDCl_3$, 298 K): δ = 2.50 (s, 3H, $-CH_3$), 2.56 (s, 3H, $-CH_3$), 2.60 (s, 6H, $-CH_3$), 7.45−7.49 (m, 9H), 7.94−8.03 (m, 6H), 8.15 (d, *J* = 5.0 Hz, 1H), 8.28 (d, *J* = 5.0 Hz, 1H), 8.58 (d, *J* = 4.5 Hz, 1H), 8.67−8.90 (m, 3H), 9.53 (s, 1H); ^1H NMR (500 MHz, $CDCl_3$, 228 K): δ = −0.39 (s, 1H, −22NH), 2.49 (s, 3H, $-CH_3$), 2.57 (s, 3H, $-CH_3$), 2.60 (s, 6H, $-CH_3$), 7.36−7.72 (m, 12H), 8.19−8.35 (m, 5H), 8.52 (s, 1H), 8.66−8.76 (m, 4H), 9.53 (s, 1H); ^{13}C NMR (125 MHz, $CDCl_3$, 298 K): δ = 21.43, 21.44, 21.5, 105.2, 120.9, 121.1, 123.4, 127.5, 127.6, 127.7, 127.9, 128.5, 129.3, 131.3, 131.5, 132.5, 133.2, 134.0, 134.1, 134.2, 134.6, 134.9, 136.2, 136.4, 138.1, 138.37, 138.42, 138.9, 139.2, 141.0, 141.6, 143.4, 148.2, 153.4, 167.1. UV−vis ($CHCl_3$): λ_{max}/nm (log ε) = 439(5.06), 534(4.05), 572(4.00), 620(3.61), 682(3.93). HRMS (ESI-TOF) calc. for $[C_{49}H_{37}N_4O]^+$ (M+H) *m*/*z* = 697.2962, Found: 697.2973.

Selected Data for ***2c***. ^1H NMR (600 MHz, $CDCl_3$, 300 K) δ = −0.17 (b, 1H), 3.81 (b, 3H), 3.936 (s, 6H), 3.944 (s, 6H), 4.04 (b, 3H), 6.77 (t, ^4J = 2.2 Hz, 1H), 6.84 (t, ^4J = 2.2 Hz, 1H), 6.885 (t, ^4J = 2.2 Hz, 1H), 6.876 (t, ^4J = 2.2 Hz, 1H), 6.95 (b, 1H), 7.35 (b, 2H), 7.73 (b, 1H), 8.30 (d, ^3J = 4.7 Hz, 1H), 8.44 (d, ^3J = 4.7 Hz, 1H), 8.71 (d, ^3J = 4.7 Hz, 1H), 8.81 (d, ^3J = 5.1 Hz, 1H), 8.82 (d, ^3J = 4.7 Hz, 1H), 8.89 (d, ^3J = 5.1 Hz, 1H), 9.72 (s, 1H); ^1H NMR (600 MHz, $CDCl_3$, 213 K) δ = −0.46 (b, 1H), 3.82 (s, 6H), 3.89 (s, 3H), 3.92 (s, 3H), 4.02 (s, 3H), 4.04 (s, 3H), 4.06 (s, 3H), 4.07 (s, 3H), 6.77 (t, ^4J = 2.2 Hz, 1H), 6.81 (m, 1H), 6.84 (t, ^4J = 2.2 Hz, 1H), 6.87 (t, ^4J = 2.2 Hz, 1H), 6.88 (t, ^4J = 2.2 Hz, 1H), 6.97 (m, 2H), 7.13 (m, 1H), 7.57 (m, 1H), 7.64 (m, 1H), 7.72 (m, 1H), 7.81 (m, 1H), 8.30 (d, ^3J = 4.6 Hz, 1H), 8.43 (d, ^3J = 4.6 Hz, 1H), 8.77 (d, ^3J = 4.6 Hz, 1H), 8.83 (d, ^3J = 5.1 Hz, 1H), 8.87 (d, ^3J = 4.6 Hz, 1H), 8.88 (d, ^3J = 5.1 Hz, 1H), 9.68 (s, 1H). ^{13}C NMR (150 MHz, $CDCl_3$, 300 K) δ_C = 55.59, 55.65, 55.71, 100.5, 100.58, 100.63, 100.7, 100.9, 105.3, 112.8, 113.1, 113.7, 114.1, 120.9, 121.3, 123.2, 127.2, 127.6, 128.6, 131.3, 131.5, 131.5, 133.2, 134.2, 135.8, 137.2, 139.3, 140.9, 141.0, 143.0, 143.5, 145.5, 147.9, 152.4, 153.3, 153.5, 158.7, 158.9, 159.0, 159.2, 159.7, 160.5, 167.4. UV−vis ($CHCl_3$) λ_{max}/nm (log ε) = 281 (4.50), 443 (5.04), 533 (4.07), 571 (4.01), 419 (3.65), 680 (3.84). HRMS (ESI-TOF) calc. for $[C_{53}H_{45}N_4O_9]^+$ (M+H) *m*/*z* = 881.3181. Found 881.3134.

Selected Data for ***2d***. ^1H NMR (500 MHz, $CDCl_3$, 298 K) δ = 3.81−4.17 (m, 36H), 7.01 (s, 1H), 7.41−7.49 (m, 6H), 7.81 (s, 1H), 8.33 (d, *J* = 4.5 Hz, 1H), 8.47 (d, *J* = 4.5 Hz, 1H), 8.76 (d, *J* = 4.5 Hz, 1H), 8.87 (t, *J* = 5.5 Hz, 2H), 8.91 (d, *J* = 5.5 Hz, 1H), 9.72 (s, 1H); ^{13}C NMR (125 MHz, $CDCl_3$, 298 K): δ = 56.3, 56.4, 56.5, 56.7, 61.1, 61.3, 61.4, 105.3, 111.9, 112.6, 112.8, 121.0, 121.4, 123.4, 127.68, 127.73, 127.6, 127.7, 128.9, 130.7, 131.4, 131.7, 131.9, 133.2, 134.2, 134.6, 136.1, 137.2, 138.3, 138.54, 138.57, 138.63, 139.3, 139.4, 141.4, 143.4, 148.0, 151.5, 151.9, 152.4, 153.2, 153.5, 153.6, 167.3. UV−vis ($CHCl_3$): λ_{max}/nm (log ε) = 447 (4.99), 535 (4.10), 575 (4.03), 625 (3.73), 682 (3.89). HRMS (ESI-TOF) calc. for $[C_{57}H_{53}N_4O_{13}]^+$ (M+H) *m*/*z* = 1001.3604, Found 1001.3615.

Synthesis of the Externally Fused Systems 4c and 4d. Solution containing 0.015 mmol of **2c** or **2d** and 40 μL (0.3 mmol) of trifluoracetic acid in toluene was heated to boiling and refluxed for 20 min. After that time, the solution was cooled to room temperature and deacidified with a few drops of aqueous sodium carbonate. The solvents were then evaporated and the residual solid was dissolved in dichloromethane and subjected to basic alumina column (Brockmann III) with dichloromethane as eluent. The first purple fraction was collected, precipitated with hexane in the form of dark red powder, and dried *in vacuo*. Yields: 9.5 mg (70%) for **4c** and 9.4 mg (63%) for **4d**.

Selected Data for ***4c***. ^1H NMR (600 MHz, $CDCl_3$, 300 K) δ = 0.76 (b, 1H, 22-NH), 3.81 (s, 3H, OMe), 3.88 (b, 3H, OMe), 3.92 (s, 6H, OMe), 3.99 (s, 6H, OMe), 4.00 (b, 3H, OMe), 4.08 (s, 6H, OMe), 6.09 (d, ^4J = 1.8 Hz, 1H, 5-*p*), 6.68 (t, ^4J = 2.2 Hz, 1H, *p*), 6.801 (t, ^4J = 2.2 Hz, 1H, *p*), 6.804 (t, ^4J = 2.3 Hz, 1H, *p*), 6.91 (b, 1H), 7.00 (dd, ^4J = 2.3 Hz, ^4J = 2.0 Hz 1H, *o*), 7.27 (d, ^4J = 2.0 Hz, 2H, *o*), 7.30 (d, ^4J = 1.8 Hz, 1H, 5-*o*′), 7.45 (dd, ^4J = 2.2 Hz, ^4J = 1.9 Hz, 1H, *o*), 7.46 (b, 1H), 7.87 (d, ^3J = 4.6 Hz, 1H, 13), 7.92 (d, ^3J = 4.6 Hz, 1H, 12), 8.27, 8.30 (d, ^3J = 4.9 Hz, 1H, 17), 8.50 (d, ^3J = 4.9 Hz, 1H, 8), 8.85 (d, ^3J = 4.9 Hz, 1H, 7). ^1H NMR (600 MHz, $CDCl_3$, 233 K) δ = 0.61 (dd, ^4J = 2.2 Hz, ^4J = 1.9 Hz, 1H, 22-NH), 3.80 (s, 3H, OMe), 3.88 (s, 3H, OMe), 3.92 (b, 6H), 3.999 (s, 3H, OMe), 4.004 (s, 3H, OMe), 4.01 (s, 3H, OMe), 4.03 (s, 3H, OMe), 6.06 (d, ^4J = 1.7 Hz, 1H, 5-*p*), 6.67 (t, ^4J = 2.2 Hz, 1H, *p*), 6.79 (t, ^4J = 2.2 Hz, 2H, *p*), 6.88 (dd, ^4J = 2.3 Hz, ^4J = 2.0 Hz 1H, *o*), 6.98 (dd, ^4J = 2.2 Hz, ^4J = 2.1 Hz 1H, *o*), 7.27 (d, ^4J = 1.7 Hz, 1H, 5-*o*), 7.456 (dd, ^4J = 2.3 Hz, ^4J = 2.0 Hz 1H, *o*), 7.463 (dd, ^4J = 2.3 Hz, ^4J = 2.2 Hz 1H, *o*), 7.87 (d, ^3J = 4.6 Hz, 1H, 13), 7.91 (d, ^3J = 4.6 Hz, 1H, 12), 8.25 (d, ^3J = 5.0 Hz, 1H, 18), 8.30 (d, ^3J = 5.0 Hz, 1H, 17), 8.54 (dd, ^3J = 4.8 Hz, ^4J = 1.9 Hz 1H, 8), 8.86 (dd, ^3J = 4.8 Hz, ^4J = 2.2 Hz 1H, 7). ^{13}C NMR (150 MHz, $CDCl_3$, 300 K) δ_C = 55.60, 55.64, 55.69, 55.73, 55.8, 56.3, 97.9, 100.57, 100.65, 100.8, 108.2, 110.4, 112.4, 112.7, 114.3, 116.9, 120.7, 122.2, 122.6, 124.4, 126.8, 127.5, 129.6, 129.7, 132.6, 135.1, 135.9, 136.4, 136.5,

dx.doi.org/10.1021/jo500272t | J. Org. Chem. 2014, 79, 3129−3139

139.6, 140.6, 140.9, 141.2, 145.1, 149.5, 156.3, 158.0, 158.6, 159.2, 159.3, 159.8, 160.5, 165.7, 182.4. HRMS (ESI-TOF)calc. for $[C_{53}H_{43}N_4O_9]^+$ (M+H) m/z = 879.3025. Found: 879.3037. UV−vis ($CHCl_3$) λ_{max}/nm (log ε) = 270 (4.46) 311(4.50), 406 (4.55), 442 (sh), 509 (4.56), 538 (4.70), 784 (3.36), 838 (3.25).

Selected Data for ***4d***. ^{1}H NMR (500 MHz, $CDCl_3$, 300 K, TMS): δ = 0.98 (b, 1H), 3.82 (s, 3H), 3.92 (s, 3H), 3.93 (b, 3H), 3.98 (s, 6H), 4.02 (s, 3H, 4.05 (s, 3H), 4.06 (b, 3H), 4.09 (s, 3H), 4.10 (s, 3H), 4.13 (s, 3H), 4.47 (s, 3H), 7.04 (b, 1H), 7.06 (s, 1H), 7.386 (s, 1H), 7.388 (d, ^4J = 1.6 Hz, 2H) 7.50 (b, 1H), 7.54 (d, ^4J = 1.7 Hz 1H), 7.85 (d, ^3J = 4.6 Hz, 1H), 7.90 (d, ^3J = 4.6 Hz, 1H), 8.26 (d, ^3J = 5.0 Hz, 1H), 8.35(d, ^3J = 5.0 Hz, 1H), 8.48 (dd, ^3J = 4.8 Hz, ^4J = 1.1 Hz, 1H), 8.80 (dd, ^3J = 4.8 Hz, ^4J = 1.1 Hz, 1H). ^{13}C NMR (150 MHz, $CDCl_3$, 300 K): δ_C = 56.3, 56.5, 61.2, 61.4, 107.3, 110.1, 112.0, 112.2, 113.0, 120.7, 120.9, 122.9, 123.8, 127.4, 127.5, 129.4, 129.7, 129.9, 132.9, 135.0, 135.1, 135.6, 136.4, 138.4, 138.7, 138.9, 140.2, 141.4, 142.7, 149.9, 151.7, 151.9, 152.5, 153.1, 153.2, 156.7, 157.1,158.5,182.2. UV−vis ($CHCl_3$, 298 K): λ/nm (log ε) = 309 (4.49), 410 (4.58), 450 (sh), 518 (sh), 541 (4.62), 632 (3.67), 721(3.28), 806 (3.21); HRMS (ESI-TOF) calc. for $C_{57}H_{50}N_4O_{13}$, m/z = 999.3447 ($[M+H]^+$). Found: 999.3428. UV−vis ($CHCl_3$, 298 K): λ/nm (ε /M^{-1} cm^{-1}) = 309 (31323), 410 (37746), 450 (sh), 518 (sh), 541 (42032), 632 (4671), 721(1930), 806 (2038).

Crystallographic Data. X-ray diffraction data of single crystals were collected at 100 K. The structures were solved by direct methods with SHELXS97[50] and refined by the full-matrix least-squares method on all F^2 data using the SHELXL97[50] programs. All H atoms, including those located in the difference density map were placed in calculated positions and refined as the riding model with Uiso(H) = 1.2Ueq(C).

*X-ray Quality Crystals of rac-***2b** *Were Obtained by Slow Diffusion of Chloroform Solution into Methanol. Crystal Data for rac-***2b**. $C_{49}H_{34}N_4O.CH_3OH$, M_r = 722.81, T = 100(2) K, Cu $K\alpha$ radiation, monoclinic, space group $P21/c$, a = 14.6447(15) Å, b = 8.4919(7) Å, c = 15.4380(11) Å, α = 90.00°, β = 94.180(8)°, γ = 90.00°, V = 1914.8(3) Å^3, Z = 2, D_c = 1.254 Mg m^{-3}, λ = 1.54178 Å, μ = 0.608 mm^{-1}, 5.75° ≤ θ ≤ 65.61°, 6182 collected reflections, 3184 independent reflections, 278 parameters, $R_1(F)$ = 0.084, $wR_2(F^2)$ = 0.2374, S = 1.130, largest difference peak and hole 0.431 and −0.409 e·Å^{-3}. The asymmetric unit consists of a half of the molecule **2b** and a molecule of methanol disordered into three sites.

*X-ray Quality Crystals of S-***2b** *Were Obtained by Slow Diffusion of Ethyl Acetate Solution into Hexane. Crystal Data for S-***2b**. $C_{49}H_{34}N_4O$, M_r = 694.80, T = 100(2) K, Cu $K\alpha$ radiation, monoclinic, space group $P21/c$, a = 14.5162(12) Å, 8.5913(10) Å, c = 15.4670(14) Å, α = 90.00°, β = 94.824(7)°, γ = 90.00°, V = 1922.1(3) Å^3, Z = 2, D_c = 1.201 Mg m^{-3}, λ = 1.54178 Å, μ = 0.564 mm^{-1}, 3.05° ≤ θ ≤ 72.42°, 9229 collected reflections, 3735 independent reflections, 253 parameters, $R_1(F)$ = 0.0987, $wR_2(F^2)$ = 0.2296, S = 1.445, largest difference peak and hole 0.593 and −0.424 e·Å^{-3}. The asymmetric unit consists of a half of the molecule **2b**.

■ ASSOCIATED CONTENT

Supporting Information

Crystallographic data in cif format, details of synthesis optimization (Table S1), calculation details (Table S2), Cartesian coordinates for the optimized structure (Table S3), calculated electronic transitions (Table S4), 1D and 2D NMR, mass spectra, and HPLC profiles. This material is available free of charge via the Internet at http://pubs.acs.org.

■ AUTHOR INFORMATION

Corresponding Authors

*E-mail: lixiaofang@iccas.ac.cn.
*E-mail: piotr.chmielewski@chem.uni.wroc.pl.

Notes

The authors declare no competing financial interest.

■ ACKNOWLEDGMENTS

This work was supported by National Natural Science Foundation of China (No. 21371054), the Scientific Research Fund of Hunan Provincial Education Department (No. 13A026), and by Polish National Science Center (Grants 2012/04A/ST5/00593 and 2013/09/B/ST5/00326). Quantum chemical calculations were performed in the Wrocław Center for Networking and Supercomputing.

■ REFERENCES

(1) Lindsey, J. S. Synthesis of *meso*-Substituted Porphyrins. In *The Porphyrin Handbook*; Kadish, K. M., Smith, K. M., Guilard, R., Eds.; Academic Press: San Diego, CA, 2000; pp 45−118.
(2) Smith, K. M. Strategies for the Synthesis of Octaalkylporphyrin Systems. In *The Porphyrin Handbook*; Kadish, K. M., Smith, K. M., Guilard, R., Eds.; Academic Press: San Diego, CA, 2000; pp 1−43.
(3) da Graça H. Vicente, M. Reactivity and Functionalization of *β*-Substituted Porphyrins and Chlorins. In *The Porphyrin Handbook*; Kadish, K. M., Smith, K. M., Guilard, R., Eds.; Academic Press: San Diego, CA, 2000; pp 149−199.
(4) Senge, M. O. Highly Substituted Porphyrins. In *The Porphyrin Handbook*; Kadish, K. M., Smith, K. M., Guilard, R., Eds.; Academic Press: San Diego, CA, 2000; pp 239−347.
(5) (a) Chou, J.-H.; Nalwa, H. S.; Kosal, M. E.; Rakow, N. A.; Suslick, K. S. Applications of Porphyrins and Metalloporphyrins to Materials Chemistry. In *The Porphyrin Handbook*; Kadish, K. M., Smith, K. M., Guilard, R., Eds.; Academic Press: San Diego, CA, 2000; pp 43−131. (b) Jiang, J. Advances in Functional Phthalocyanine Materials. In *Structural Bonding (Berlin)*, Heidelberg: Springer-Verlag, 2010. (c) Jiang, J.; Ng, D. K. P. *Acc. Chem. Res.* **2009**, *42*, 79−88.
(6) Aida, T.; Inoue, S. Metalloporphyrins as Catalysts for Precision Macromolecular Synthesis. In *The Porphyrin Handbook*; Kadish, K. M., Smith, K. M., Guilard, R., Eds.; Academic Press: San Diego, CA, 2000; pp 133−156.
(7) Pandey, R. K.; Zheng, G. Porphyrins as Photosensitizers in Photodynamic Therapy. In *The Porphyrin Handbook*; Kadish, K. M., Smith, K. M., Guilard, R., Eds.; Academic Press: San Diego, CA, 2000; pp 157−230.
(8) Malinski, T. Porphyrin-Based Electrochemical Sensors. In *The Porphyrin Handbook*; Kadish, K. M., Smith, K. M., Guilard, R., Eds.; Academic Press: San Diego, CA, 2000; pp 231−256.
(9) Ogoshi, H.; Mizatuni, T.; hayashi, T.; Kuroda, Y. Porphyrins and Metalloporphyrins as Receptor Models in Molecular Recognition. In *The Porphyrin Handbook*; Kadish, K. M., Smith, K. M., Guilard, R., Eds.; Academic Press: San Diego, CA, 2000; pp 279−340.
(10) Chmielewski, P. J.; Latos-Grażyński, L.; Rachlewicz, K.; Głowiak, T. *Angew. Chem., Int. Ed. Engl.* **1994**, *33*, 779−781.
(11) Furuta, H.; Asano, T.; Ogawa, T. *J. Am. Chem. Soc.* **1994**, *116*, 767−768.
(12) Geier, G. R., III; Haynes, D. M.; Lindsey, J. S. *Org. Lett.* **1999**, *1*, 1455−1458.
(13) Latos-Grażyński, L. Core Modified Heteroanalogues of Porphyrins and Metalloporphyrins. In *The Porphyrin Handbook*; Kadish, K. M., Smith, K. M., Guilard, R., Eds.; Academic Press: New York, 2000; pp 361−416.
(14) Chmielewski, P. J.; Latos-Grażyński, L. *Coord. Chem. Rev.* **2005**, *249*, 2510−2533.
(15) Toganoh, M.; Furuta, H. *Chem. Commun.* **2012**, *48*, 937−954.
(16) Maeda, H.; Furuta, H. *Pure Appl. Chem.* **2006**, *78*, 29−44.
(17) Srinivasan, A.; A Furuta, H. *Acc. Chem. Res.* **2005**, *38*, 10−20.
(18) Chmielewski, P. J.; Schmidt, I. *Inorg. Chem.* **2004**, *43*, 1885−1894.
(19) Chmielewski, P. J. *Inorg. Chem.* **2007**, *46*, 1617−1626.
(20) Siczek, M.; Chmielewski, P. J. *Angew. Chem., Int. Ed.* **2007**, *46*, 7432−7436.
(21) Chmielewski, P. J.; Durlej, B.; Siczek, M.; Szterenberg, L. *Angew. Chem., Int. Ed.* **2009**, *48*, 8736−8739.
(22) Chmielewski, P. J.; Szterenberg, L.; Siczek, M. *Chem.—Eur. J.* **2011**, *17*, 1009−1020.

(23) Chmielewski, P. J.; Maciołek, J. *Chem. Commun.* **2012**, *48*, 428−430.
(24) Li, X.; Liu, B.; Yu, X.; Yi, P.; Yi, R.; Chmielewski, P. J. *J. Org. Chem.* **2012**, *77*, 2431−2440.
(25) Li, X.; Liu, B.; Xu, X.; Chmielewski, P. J. *J. Org. Chem.* **2012**, *77*, 8206−8219.
(26) Liu, B.; Li, X.; Xu, X.; Stępień, M.; Chmielewski, P. *J. Org. Chem.* **2013**, *78*, 1354−1364.
(27) Kashiwagi, N.; Akeda, T.; Morimoto, T.; Ishizuka, T.; Furuta, H. *Org. Lett.* **2007**, *9*, 1733−1736.
(28) Toganoh, M.; Kimura, T.; Furuta, H. *Chem. Commun.* **2008**, 102−104.
(29) Toganoh, M.; Kimura, T.; Furuta, H. *Chem.—Eur. J.* **2008**, *14*, 10585−10594.
(30) Grzegorzek, N.; Pawlicki, M.; Latos-Grażyński, L. *J. Org. Chem.* **2009**, *74*, 8547−8553.
(31) Toganoh, M.; Hihara, T.; Furuta, H. *Inorg. Chem.* **2010**, *49*, 8182−8184.
(32) Seybold, P. G.; Gouterman, M. *J. Mol. Spectrosc.* **1969**, *31*, 1−13.
(33) Wolff, S. A.; Alemán, E. A.; Banerjee, D.; Rinaldi, P. L.; Modarelli, D. *J. Org. Chem.* **2004**, *69*, 4576.
(34) Chmielewski, P. J.; Siczek, M.; Szterenberg, L. *Inorg. Chem.* **2011**, *50*, 6719−6736.
(35) Cao, W.; Wang, H.; Wang, X.; Lee, H. K.; Ng, D. K. P.; Jiang, J. *Inorg. Chem.* **2012**, *51*, 9265−9272.
(36) Wann, S. R.; Thorsen, P. T.; Kreevoy, M. M. *J. Org. Chem.* **1981**, *46*, 2579−2581.
(37) Chmielewski, P. J.; Maciołek, J.; Szterenberg, L. *Eur. J. Org. Chem.* **2009**, 3930−3939.
(38) March, J. *Advanced Organic Chemistry*; Wiley and Sons: New York, 1992.
(39) McClelland, R. A. *J. Am. Chem. Soc.* **1975**, *97*, 5281−5282.
(40) Bennet, A. J.; Ślebocka-Tilk, H.; Brown, R. S.; Guthrie, J. P.; Jodhan, A. *J. Am. Chem. Soc.* **1990**, *112*, 8497−8506.
(41) Myśliwiec, D.; Donnio, B.; Chmielewski, P. J.; Heinrich, B.; Stępień, M. *J. Am. Chem. Soc.* **2012**, *134*, 4822−4833.
(42) Frisch, M. J.; Trucks, G. W.; Schlegel, H. B.; Scuseria, G. E.; Robb, M. A.; Cheeseman, J. R.; Scalmani, G.; Barone, V.; Mennucci, B.; Petersson, G. A.; Nakatsuji, H.; Caricato, M.; Li, X.; Hratchian, H. P.; Izmaylov, A. F.; Bloino, J.; Zheng, G.; Sonnenberg, J. L.; Hada, M.; Ehara, M.; Toyota, K.; Fukuda, R.; Hasegawa, J.; Ishida, M.; Nakajima, T.; Honda, Y.; Kitao, O.; Nakai, H.; Vreven, T. Montgomery, Jr., J. A.; Peralta, J. E.; Ogliaro, F.; Bearpark, M.; Heyd, J. J.; Brothers, E.; Kudin, K. N.; Staroverov, V. N.; Keith, T.; Kobayashi, R.; Normand, J.; Raghavachari, K.; Rendell, A.; Burant, J. C.; Iyengar, S. S.; Tomasi, J.; Cossi, M.; Rega, N.; Millam, J. M.; Klene, M.; Knox, J. E.; Cross, J. B.; Bakken, V.; Adamo, C.; Jaramillo, J.; Gomperts, R.; Stratmann, R. E.; Yazyev, O.; Austin, A. J.; Cammi, R.; Pomelli, C.; Ochterski, J. W.; Martin, R. L.; Morokuma, K.; Zakrzewski, V. G.; Voth, G. A.; Salvador, P.; Dannenberg, J. J.; Dapprich, S.; Daniels, A. D.; Farkas, O.; Foresman, J. B.; Ortiz, J. V.; Cioslowski, J.; and Fox, D. J. *Gaussian 09*, revision B.01; Gaussian, Inc., Wallingford, CT, 2010.
(43) Becke, A. D. *Phys. Rev. A* **1988**, *38*, 3098−3100.
(44) Becke, A. D. *J. Chem. Phys.* **1993**, *98*, 5648.
(45) Lee, C.; Yang, W.; Parr, R. G. *Phys. Rev. B* **1988**, *37*, 785−789.
(46) Wadt, W. R.; Hay, P. J. *J. Chem. Phys.* **1985**, *82*, 284−298.
(47) Hay, P. J.; Wadt, W. R. *J. Chem. Phys.* **1985**, *82*, 299−310.
(48) O'Boyle, N. M.; Tenderholt, A. L.; Langner, K. M. *J. Comput. Chem.* **2008**, *29*, 839−845.
(49) Liu, B.; Li, X.; Zhang, J.; Chmielewski, P. J. *Org. Biol. Chem.* **2013**, *11*, 4831−4839.
(50) Sheldrick, G. M. *Acta Crystallogr.* **2008**, *A64*, 112−122.